

Disk–Halo Model for Flat-Spectrum T Tauri Stars

Nobuhiro KIKUCHI

*Earth Observation Research Center, National Space Development Agency of Japan,
1-8-10 Harumi, Chuo-ku, Tokyo 104-6023
kikuchi@eorc.nasda.go.jp*

Taishi NAKAMOTO

*Center for Computational Physics, University of Tsukuba, Tsukuba, Ibaraki 305-8577
and*

Koji OGOCHI

Information Technology of Japan Inc., Mito, Ibaraki 310-0803

(Received 1999 April 23; accepted 2002 June 16)

Abstract

We explore the origin of the flat spectrum seen in some T Tauri stars by considering a three-component structure: a central star, a circumstellar disk, and a dusty halo. The radiative energy transport is faithfully treated by solving the angle- and frequency-dependent radiative transfer equation in two space dimensions assuming axisymmetry, and hence the radiative equilibrium temperature in the disk and halo is determined simultaneously. The disk is effectively heated by the scattering and reprocessing of stellar radiation through the halo. The large mid- to far-infrared excess originates from the photosphere of the warmed disk, resulting in a flat spectrum, as observed. The halo which we consider is observed as a compact reflection nebula, and is discriminated from extended, disk-like envelopes around flat-spectrum T Tauri stars. We show that the overall spectral shape of flat-spectrum T Tauri stars can be reproduced by the present *disk-halo* model.

Key words: planetary systems: protoplanetary disk — radiative transfer — stars: formation

1. Introduction

It seems reasonable to suppose that the infrared excesses of T Tauri stars can be attributed to thermal dust emission from circumstellar disks. By modeling the observed spectral energy distributions (SEDs), one can derive the disk properties, such as masses, radii, and temperature distributions (Adams et al. 1988; Strom et al. 1989; Beckwith et al. 1990). Such spectral modeling, however, has revealed an extreme class of T Tauri stars, namely flat-spectrum T Tauri stars. The large mid- to far-infrared excesses of flat-spectrum T Tauri stars require their disks to have a temperature distribution of the form $T \propto R^{-1/2}$ (Adams et al. 1988), where R is the distance from the rotation axis, whereas a $T \propto R^{-3/4}$ dependence is predicted by both a standard accretion disk (Lynden-Bell, Pringle 1974) and a spatially flat reprocessing disk (Adams, Shu 1986). This implies that the disks of flat-spectrum T Tauri stars are warmer in the outer regions than predicted by the simple disk models; we must therefore consider the mechanisms which heat the outer region of the disk. Disk flaring allows a disk to receive more emission from the central star, and to produce temperature distributions shallower than $T \propto R^{-3/4}$ (Kusaka et al. 1970; Kenyon, Hartmann 1987), but does not suffice to reproduce the observed flux.

The infrared excesses may originate from another circumstellar dust component. Calvet et al. (1994) invoked infalling envelopes, which were originally applied to the spectral modeling of protostars (Adams, Shu 1986; Kenyon et al. 1993), and showed that the infalling en-

velopes can produce the mid- to far-infrared excesses of flat-spectrum T Tauri stars. In fact, observations have shown that there exists an extended, disk-like structure of radius ~ 1000 AU around a typical flat-spectrum T Tauri star, HL Tau (Sargent, Beckwith 1991). Furthermore, Hayashi, Ohashi, and Miyama (1993) have revealed an infalling motion in the disk-like structure of HL Tau, suggesting that it is a remnant of an infalling envelope.

Although the infalling envelope model of Calvet et al. (1994) is successful in reproducing the flat spectrum, it does not take into account the following two important effects. First, as pointed out by Natta (1993), envelopes scatter and reprocess the stellar radiation toward the disk, and thereby alter the temperature distribution in the disk (see also Butner et al. 1994; D’Alessio et al. 1997). Second, the disk, itself, significantly influences the temperature distribution in the envelope. Since these two effects are coupled with each other, they cannot be treated separately. Hence, to elucidate the substantial mechanism for the flat spectrum, the temperature structure of the disk and envelope should be solved simultaneously. In the present analysis, we consistently handle the radiative energy transport in the disk and envelope by solving the angle- and frequency-dependent radiative transfer equation in two space dimensions by assuming axisymmetry.

In this paper, we demonstrate that the mid- to far-infrared excesses of flat-spectrum T Tauri stars can originate from the *disk*. Since the envelope which heats the disk can be as compact as the disk itself, we henceforth call it a *halo* to distinguish it from an extended infalling

envelope. The reflection nebula of HL Tau revealed by the Hubble Space Telescope (Stapelfeldt et al. 1995) may be regarded as an observational counterpart of the halo.

2. Model

The disk–halo model consists of a central star, a circumstellar disk, and a halo surrounding both of them. We first assume the axial and equatorial symmetry. The central star has luminosity L_* and mass M_* , and radiates as a blackbody with effective temperature T_* . We consider models with $M_* = 0.5 M_\odot$ and $T_* = 4000$ K, which are typical values for pre-main-sequence stars in the Taurus–Auriga molecular cloud. We adopt $L_* = 5 L_\odot$ for models without disk accretion, in which all the energy is radiated by the central star. Models with disk accretion are also examined, for which stellar luminosity is taken to be $L_* = 2 L_\odot$ and the disk, itself, has some intrinsic luminosity.

The surface density distribution of the disk is assumed to be a power law,

$$\sigma(R) = \sigma_1 (R/\text{AU})^{-3/2}, \quad (1)$$

in the range $1 \text{ AU} \leq R \leq 100 \text{ AU}$. Outside this range, we make the surface density go to zero smoothly inward down to $R_{\text{in}} = 0.1 \text{ AU}$ and outward up to $R_{\text{out}} = 120 \text{ AU}$. The value of σ_1 specifies the disk mass. We consider models with $\sigma_1 = 2 \times 10^3 \text{ g cm}^{-2}$, which gives $0.02 M_\odot$ for the disk mass, and is consistent with the minimum mass solar nebula (Hayashi et al. 1985). For the given surface density distribution, the two-dimensional density distribution in the disk is determined by the hydrostatic equilibrium in the vertical direction under the gravity of the central star.

In addition to the radiation from the central star, viscous dissipation also heats the disk if it is undergoing accretion, as observations of classical T Tauri stars suggest (e.g., Bertout et al. 1988). We take into account the effects of disk accretion in a simple way as follows. Assuming that the mass accretion rate in the disk, \dot{M}_d , is constant with radius, we express the energy generation rate per unit area as (Lynden-Bell, Pringle 1974)

$$D(R) = \frac{3GM_*\dot{M}_d}{4\pi R^3} \left(1 - \sqrt{\frac{R_{\text{in}}}{R}} \right) \quad (2)$$

in the range $R_{\text{in}} \leq R \leq R_{\text{out}}$. We further assume that the energy generation rate per unit mass does not depend on the vertical height, which can be written as

$$\varepsilon(R) = D(R)/\sigma(R). \quad (3)$$

The intrinsic disk luminosity is then given by integrating equation (2) over the disk area as

$$\begin{aligned} L_d &= 2\pi \int_{R_{\text{in}}}^{R_{\text{out}}} D(R) R dR \\ &= \frac{GM_*\dot{M}_d}{2R_{\text{in}}} \left[1 - 3\frac{R_{\text{in}}}{R_{\text{out}}} + 2\left(\frac{R_{\text{in}}}{R_{\text{out}}}\right)^{3/2} \right]. \end{aligned} \quad (4)$$

In a classical picture of accretion disks, the disk extends

down to the stellar radius R_* to form a boundary layer, where disk material slows down from Keplerian to stellar rotation velocity. Radiation from a boundary layer accounts for the ultraviolet and optical excesses of T Tauri stars (Lynden-Bell, Pringle 1974). On the other hand, our disk model has an inner radius of $R_{\text{in}} = 0.1 \text{ AU}$, which is well above the stellar surface. The underlying assumption for this is that the stellar magnetic field truncates the disk at several stellar radii, and accretion from the disk onto the central star takes place along the magnetic field lines (Bertout et al. 1988). A “bright spot” is then formed where the accreting material impacts the stellar surface. The luminosity of the radiation from this bright spot can be as large as the stellar luminosity, and therefore it will also be important as an additional energy source for disk heating. In our model, disk material flows at the rate \dot{M}_c from the disk inner radius onto the stellar surface, and the amount of radiation energy emitted by the bright spot is given by

$$L_c = \frac{GM_*\dot{M}_c}{R_*} - \frac{1}{2} \frac{GM_*\dot{M}_c}{R_{\text{in}}}, \quad (5)$$

which derives from the assumption that the energy difference of accreting material between the total kinetic + gravitational energy at $R = R_{\text{in}}$ and the gravitational energy at $R = R_*$ is released by radiation from the bright spot. The stellar radius, R_* , is defined by $L_* = 4\pi R_*^2 \sigma_B T_*^4$. We do not assume that \dot{M}_c is equal to \dot{M}_d , i.e., we consider models with unsteady disk accretion. For simplicity, the bright spot is assumed to radiate isotropically as a blackbody with an effective temperature of 8000 K.

The density distribution in the halo is supposed to be a power law,

$$\rho_h(r) = \rho_1 (r/\text{AU})^{-p}, \quad (6)$$

for $r \geq 1 \text{ AU}$, where r is the distance from the central star and ρ_1 is a reference density. To avoid a singularity at $r = 0$, we take $\rho_h(r) = \rho_1 [1 + p/2 - p/2(r/\text{AU})^2]$ for $r \leq 1 \text{ AU}$. A different assumption for cutting off the power-law behavior, for instance, keeping the power law down to 0.1 AU, did not change the results significantly. Since bipolar outflows may evacuate material along the rotation axis, we introduce bipolar holes with an opening half-angle of θ_{bp} . The halo density is reduced slowly and smoothly inside the bipolar holes by multiplying a factor $f_{\text{bp}} = 3(\theta/\theta_{\text{bp}})^2 - 2(\theta/\theta_{\text{bp}})^3$ to the original halo density for $\theta \leq \theta_{\text{bp}}$, where θ is the polar angle.

The frequency-dependent absorption and scattering coefficients of dust particles are taken from Miyake and Nakagawa (1993), assuming that the size distribution of dust particles, $n(a)$, with respect to the radius, a , is expressed by $n(a) \propto a^{-3.5}$ for $0.01 \mu\text{m} \leq a \leq 1 \mu\text{m}$ and $n(a) \propto a^{-5.5}$ for $1 \mu\text{m} \leq a \leq 10 \mu\text{m}$. Miyake and Nakagawa (1993) assumed that dust particles are composed of silicate and water ice. We further assume that the dust vaporization temperatures are 1000 K and 100 K for silicate and water ice, respectively. For simplicity, we adopt the approximation of isotropic scattering.

Given the density distributions and the radiative and

viscous heating sources, we calculate radiative equilibrium temperature in the disk and halo which satisfies the condition of radiative equilibrium,

$$4\pi \int_0^\infty \kappa_\nu^{\text{abs}} B_\nu(T) d\nu = c \int_0^\infty \kappa_\nu^{\text{abs}} E_\nu d\nu + \varepsilon, \quad (7)$$

where ν is the frequency, κ_ν^{abs} is the mass absorption coefficient, B_ν is the Planck function, T is the temperature, and E_ν is the monochromatic radiation energy density. To solve equation (7), we adopt the variable Eddington factor method in a cylindrical coordinate system (R, Z) (Stone et al. 1992), in which we integrate the time-dependent radiation moment equations forward in time until a stationary state is achieved. The radiation moment equations are closed by introducing variable Eddington factors, which are in turn calculated from the solution of the angle- and frequency-dependent radiative transfer equation. For every timestep, the disk is assumed to be in hydrostatic equilibrium determined by the temperature distribution at the previous timestep. Stationary state solutions obtained in this way then satisfy the conditions of radiative and hydrostatic equilibria simultaneously. We take the size of the computational box to be 200 AU \times 200 AU using a 100 \times 100 non-uniform spatial grid, and employ 203 \times 101 angle rays and 101 frequency meshes. The accuracy of our radiative transfer method has been confirmed by test calculations described in Stone et al. (1992) and in Masunaga, Miyama, and Inutsuka (1998).

3. Results

3.1. Standard Case

The halo density distribution, $\rho_h(r) = \rho_1 (r/\text{AU})^{-3/2}$, is a natural consequence of infalling material with a constant mass infall rate, \dot{M} , if ρ_1 is given by $\rho_1 = (4\pi)^{-1} \dot{M} (2GM_*)^{-1/2} (\text{AU})^{-3/2}$. From the spectral modeling of protostars in the Taurus–Auriga molecular cloud, Kenyon et al. (1993) derived a typical mass infall rate of $\dot{M} = 4 \times 10^{-6} M_\odot \text{ yr}^{-1}$, which gives $\rho_1 = 3 \times 10^{-14} \text{ g cm}^{-3}$ for $M_* = 0.5 M_\odot$. Noting this value of ρ_1 , we first present results for a halo model with $p = 3/2$, $\rho_1 = 10^{-14} \text{ g cm}^{-3}$ and $\theta_{\text{bp}} = 60^\circ$. In a standard case detailed in this subsection, disk accretion is not included, and all of the energy arises from the central star with luminosity $L_* = 5 L_\odot$.

Figure 1 shows the density and temperature distributions in the disk and halo. The temperature gradient is shallow along the axis of symmetry where the density is very low, while it is steep along the midplane where the disk is situated. The resulting temperature distribution is far from spherically symmetric, as illustrated by the contours in the teardrop shape. It can also be seen from figure 1 that the disk is not isothermal in the vertical direction, with a surface temperature higher than the midplane temperature. The vertical structure at $R = 10$ AU is shown in figure 2a. The disk surface lies at $Z \simeq 4$ AU, which is defined as the position above which the density of the disk decreases below that of the halo. As illustrated by the solid line in figure 2a, the temperature T begins to rise at $Z \simeq 1$ AU, reaches its maximal value at the disk

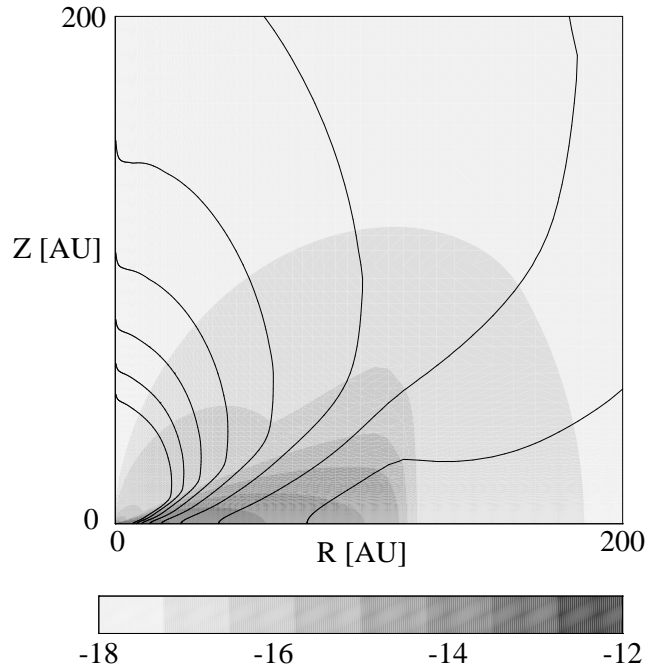


Fig. 1. Density and temperature distributions for the standard model having $\rho_1 = 1.0 \times 10^{-14} \text{ g cm}^{-3}$, $\theta_{\text{bp}} = 60^\circ$ and $p = 3/2$. The grey scale and contours represent the density and temperature, respectively. The innermost contour is $T = 100$ K, and the contours decrease outward in 10 K intervals.

surface and then decreases. This pronounced temperature rise at a disk surface can be explained by the frequency-dependence of dust-absorption coefficient. Absorption efficiency of dust particles is higher for short-wavelength radiation than for long-wavelength radiation. The disk surface, which is exposed directly to a high-temperature radiation field in the halo, is therefore warmer than the disk interior (Chiang, Goldreich 1997).

In figure 2b the brightness temperature, T_b , at frequency $\nu = 10^{13} \text{ Hz}$ is shown as a function of Z . We define T_b according to $I_\nu = 2h\nu^3/c^2 [\exp(h\nu/k_B T_b) - 1]$, where I_ν is the specific intensity, and is calculated assuming that the system is viewed pole-on. Also plotted in figure 2b is the optical depth, τ_ν , at $\nu = 10^{13} \text{ Hz}$, which is measured from $Z = 200$ AU toward the midplane. As illustrated by the dashed line in figure 2b, T_b is equal to T near the midplane where $\tau_\nu \gg 1$; as Z increases, T_b also increases along with T as long as $\tau_\nu \geq 1$. When τ_ν becomes less than unity, T_b begins to depart from T , and keeps an almost constant value in the halo. Thus, as expected, we find that the observed value of T_b is determined by the value of T at $\tau_\nu \simeq 1$. Since the halo does not have τ_ν larger than unity, we can define the “photosphere” of the disk as the position of $\tau_\nu = 1$ at mid- to far-infrared wavelengths. Then, the observed brightness temperature at mid- to far-infrared wavelengths traces the photospheric temperature of the disk.

Figure 3 shows radial distributions of the midplane temperature and the brightness temperature at $\nu = 10^{13} \text{ Hz}$

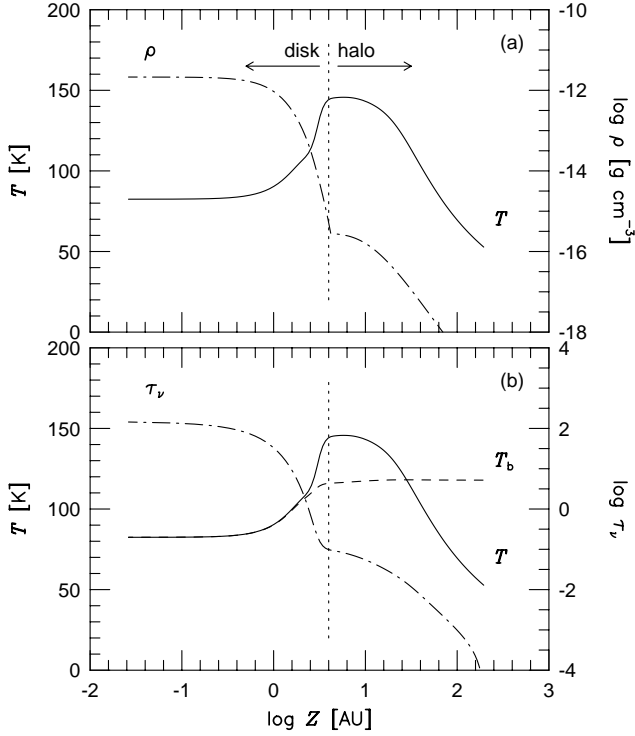


Fig. 2. Vertical structure at $R = 10$ AU for the standard model. (a) Temperature T (solid line) and density ρ (dot-dashed line) are plotted as a function of Z . (b) Temperature T (solid line), brightness temperature T_b at $\nu = 10^{13}$ Hz (dashed line), and optical depth τ_ν at $\nu = 10^{13}$ Hz (dot-dashed line) measured from $Z = 200$ AU toward the midplane are plotted as a function of Z .

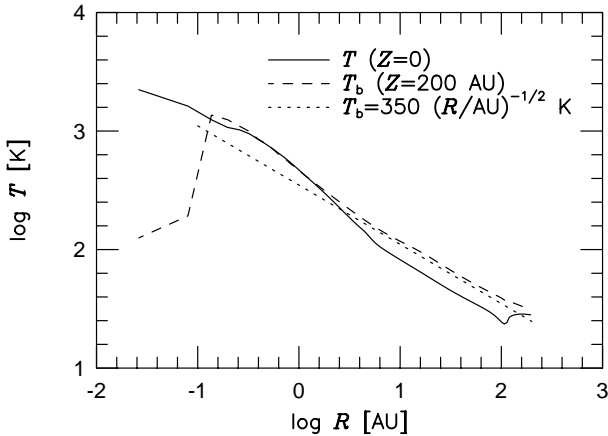


Fig. 3. Radial distributions of the midplane temperature T (solid line) and the brightness temperature T_b at $\nu = 10^{13}$ Hz (dashed line) evaluated at $Z = 200$ AU. The dotted line represents a power law $T_b(R) = 350 (R/\text{AU})^{-1/2}$ K.

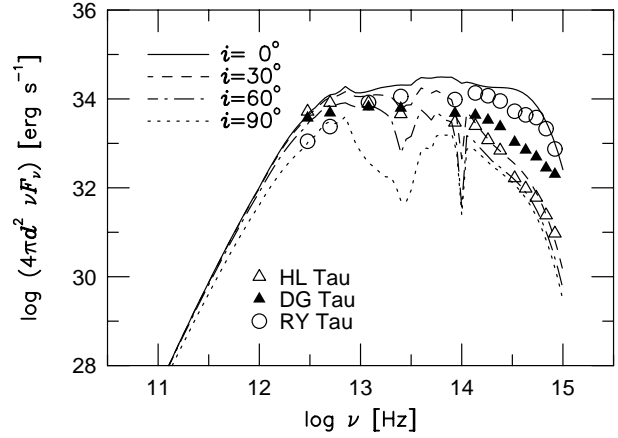


Fig. 4. Spectral energy distributions of the standard model at four viewing angles $i = 0^\circ$ (solid line), 30° (dashed line), 60° (dot-dashed line), and 90° (dotted line). The symbols represent observational data taken from Strom et al. (1989) for HL Tau (open triangles), DG Tau (solid triangles) and RY Tau (open circles).

evaluated at $Z = 200$ AU. We should be reminded that the SED is not determined by the midplane temperature, but by the brightness temperature. We find that it can be well approximated by $T_b(R) = 350 (R/\text{AU})^{-1/2}$ K in $1 \text{ AU} \leq R \leq 100 \text{ AU}$. This brightness temperature distribution is comparable to the temperature distribution $T(R) = 307 (R/\text{AU})^{-0.49}$ K, which was derived for HL Tau through spectral modeling (Beckwith et al. 1990). This comparison shows that the disk-halo model can produce the large mid- to far-infrared excess of the typical flat-spectrum T Tauri star. Moreover, from the result that the brightness temperature traces the photospheric temperature of the disk, it follows that the mid- to far-infrared excess originates from the disk.

In figure 4 the model SEDs are shown at several viewing angles. As expected from the results described above, the model SEDs are nearly flat in the infrared at viewing angles of $i = 0^\circ$ and 30° . At $i = 60^\circ$, the model SED has a weak negative slope in the infrared, with a deep absorption feature near $\lambda = 10 \mu\text{m}$ made by silicate and water ice (see Miyake, Nakagawa 1993). The water ice feature at $3.1 \mu\text{m}$ is also seen at $i = 30^\circ$ and 60° . In the optical and near-infrared, the shape of the model SED varies significantly with the viewing angle. The optical depth to the central star at V band ($\lambda = 0.55 \mu\text{m}$) is 3, 18, and 45 at $i = 10^\circ$, 30° , and 60° , respectively. Thus, the central star is highly obscured when viewed at $i = 30^\circ$ and 60° , and the optical flux is due to the scattered light.

Observational data taken from Strom et al. (1989) for three flat-spectrum T Tauri stars (HL Tau, DG Tau, and

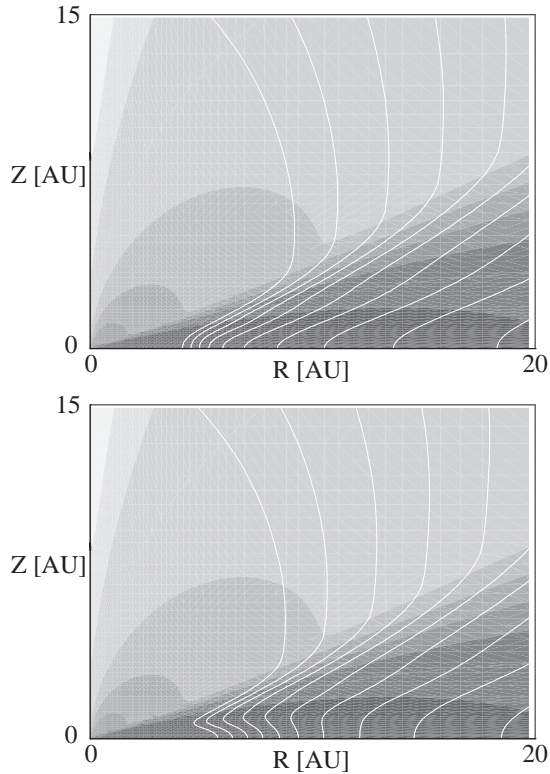


Fig. 5. Closeup view of the density and temperature distributions to the center for the standard model (upper panel) and for the steady accretion model (lower panel). For both models, the innermost contour is $T = 150$ K, and contours decrease outward in 10 K intervals.

RY Tau) are also plotted in figure 4, assuming that the distance to these sources is $d = 140$ pc. Compared with the observational data, we find that the model SEDs can reproduce the overall spectral shape of these sources, although the model parameters are not tuned for any specific object.

3.2. Effects of Disk Accretion

In this subsection we examine the effects of disk accretion on the temperature distribution and the SED. The stellar luminosity is taken to be $L_* = 2 L_\odot$, and the disk accretion is assumed to contribute to a substantial fraction of the total luminosity. We first consider a steady accretion model, i.e., the accretion rate in the disk is equal to that from the disk onto the star. From analyses of the ultraviolet and optical excesses, the accretion rate has been estimated to be in the range $5 \times 10^{-8} - 5 \times 10^{-7} M_\odot \text{ yr}^{-1}$ for classical T Tauri stars (Bertout et al. 1988). Hence,

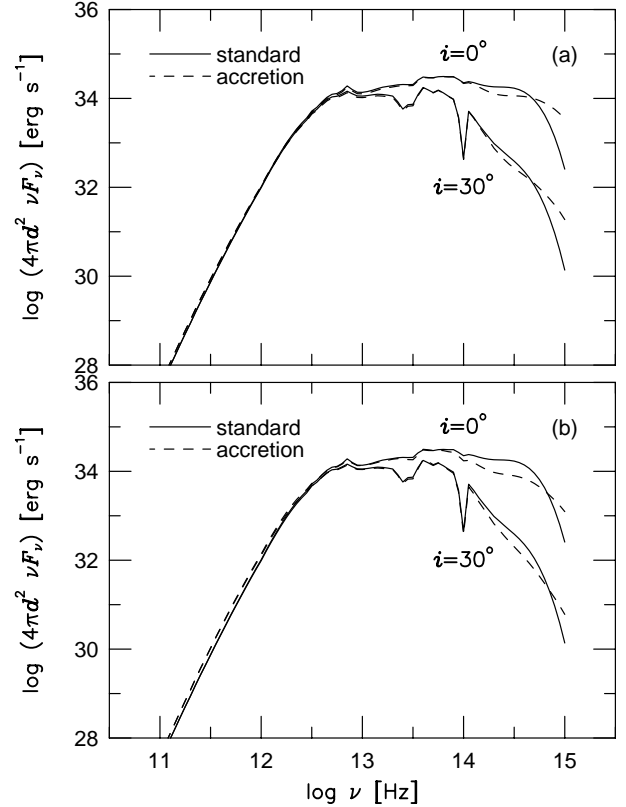


Fig. 6. Effects of disk accretion on the SED. The results are shown at two viewing angles, $i = 0^\circ$ and 30° . (a) Comparison of the steady accretion model (dashed line) with the standard model (solid line). (b) Comparison of the unsteady accretion model (dashed line) with the standard model (solid line).

we adopt $\dot{M}_d = \dot{M}_c = 5 \times 10^{-7} M_\odot \text{ yr}^{-1}$ for the steady accretion model. From equations (4) and (5), one obtains accretion luminosities of $L_d = 0.18 L_\odot$ for the disk and $L_c = 2.46 L_\odot$ for the bright spot, respectively. The total luminosity is then $4.65 L_\odot$, which is almost the same as that of the standard model discussed in the previous subsection, and thus it is possible to directly compare models with and without disk accretion.

Figure 5 shows a closeup view of the density and temperature distributions to the center for the standard model (upper panel) and for the steady accretion model (lower panel). In the standard model, the temperature distribution is determined entirely by radiative transport of energy emitted by the central star, and the temperature monotonically increases along the vertical direction in the disk. On the other hand, the steady accretion model shows a more complicated temperature structure in the disk. Inside ~ 10 AU, the temperature is higher at the midplane in the steady accretion model than in the standard model, indicating that viscous dissipation effectively heats the disk in this region. Although the temperature decreases along the vertical direction to transport radiatively the energy generated by viscous dissipation, it rises again toward the disk surface as in the standard model.

Note that the temperature distribution of the steady accretion model is quite similar to that of the standard model in the halo and the disk outside ~ 10 AU, suggesting that viscous dissipation is not an important heating source in these regions.

Figure 6 compares the SEDs of models with and without disk accretion. As discussed in the previous subsection, the mid- to far-infrared portion of the SED is determined mainly by the photospheric temperature of the outer disk. It can be seen from figure 6a that the SED of the steady accretion model does not differ significantly from that of the standard model in the mid- to far-infrared region. Therefore, the photospheric temperature of the outer disk is determined by the radiation energy from the central star and the bright spot, not by viscous dissipation in the disk. The radiation energy source of the standard model is a 4000 K blackbody with $5 L_{\odot}$, while that of the steady accretion model is a combination of two blackbodies with different temperatures. The difference in the radiation energy spectra appears in the ultraviolet and optical portions of the SED. Compared with the standard model, the steady accretion model shows more ultraviolet and less optical fluxes. The result shown in figure 6a indicates that the mid- to far-infrared portion of the SED, and hence the photospheric temperature of the disk, is not sensitive to the spectrum of the central radiation energy source. This is because the inner region of the halo immediately scatters or absorbs/reradiates radiation from the center at longer wavelengths.

We next consider a model in which accretion takes place unsteadily, in the sense that the disk accretion rate is constant in radius, but it is not equal to the rate at which disk material flows from the inner edge onto the central star. The possibility that accretion flow in HL Tau is unsteady was discussed by Lin et al. (1994). The flattened envelope around HL Tau is inferred to accrete dynamically onto the disk at a rate of $5 \times 10^{-6} M_{\odot} \text{ yr}^{-1}$, while the accretion rate from the disk onto the central star should be smaller than $7 \times 10^{-7} M_{\odot} \text{ yr}^{-1}$, because the accretion luminosity cannot be larger than the total luminosity of HL Tau (Lin et al. 1994). In the unsteady accretion model considered here, we adopt $\dot{M}_d = 5 \times 10^{-6} M_{\odot} \text{ yr}^{-1}$, which gives an intrinsic disk luminosity of $L_d = 1.81 L_{\odot}$. The accretion rate from the disk onto the central star is taken to be $\dot{M}_c = 2 \times 10^{-7} M_{\odot} \text{ yr}^{-1}$, which is one order magnitude smaller than \dot{M}_d , and produces a bright-spot luminosity of $L_c = 0.99 L_{\odot}$. The total luminosity then becomes $4.80 L_{\odot}$, which is also comparable to that of the standard model.

Figure 6b shows SEDs for the standard and unsteady accretion models. Comparing these two models, we find no significant difference in the mid- to far-infrared portion of the SED. The unsteady accretion model, however, emits more ultraviolet and less optical flux, which may be attributed to the difference in the spectra of the central radiation energy sources. This feature is similar to that seen in the steady accretion model. In the unsteady accretion model, however, the central star and bright spot emit only about $3 L_{\odot}$ to heat the disk, which would not

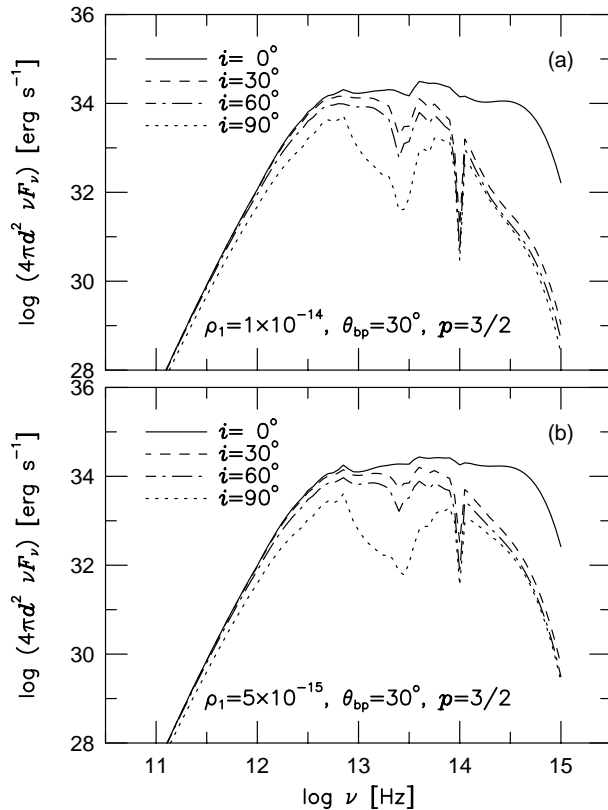


Fig. 7. Effects of the size of the bipolar lobes on the SED. (a) SEDs for a model with $\rho_1 = 1.0 \times 10^{-14} \text{ g cm}^{-3}$, $\theta_{\text{bp}} = 30^\circ$, and $p = 3/2$. (b) SEDs for a model with $\rho_1 = 5.0 \times 10^{-15} \text{ g cm}^{-3}$, $\theta_{\text{bp}} = 30^\circ$, and $p = 3/2$.

be sufficient to produce a mid- to far-infrared flux as large as that of the standard or steady accretion model. This deficit of radiation energy is compensated by the accretion energy generated in the innermost region of the disk. In general, most of the accretion energy is released in the innermost region of the system where the gravitational potential well is deep. In the unsteady accretion model we adopt, equation (2) indicates that 80% of the intrinsic disk luminosity is generated inside 1.2 AU. The accretion energy released in the innermost region of the disk is radiated at short wavelengths. This emission is subsequently scattered or absorbed and reradiated by the halo to heat the outer region of the disk, producing the large mid- to far-infrared excess, as shown in figure 6b.

Figure 6b also shows that the unsteady accretion model produces more flux at radio wavelengths than the standard model. At radio wavelengths, our disk model is optically thin, and thus the emergent flux is related to the temperature at the midplane where disk material is concentrated. Our result indicates that, for a fixed total luminosity, disk accretion at a rate as high as $5 \times 10^{-6} M_{\odot} \text{ yr}^{-1}$ can increase the radio flux by increasing the midplane temperature, although it does not modify the mid- to far-infrared portion of the SED.

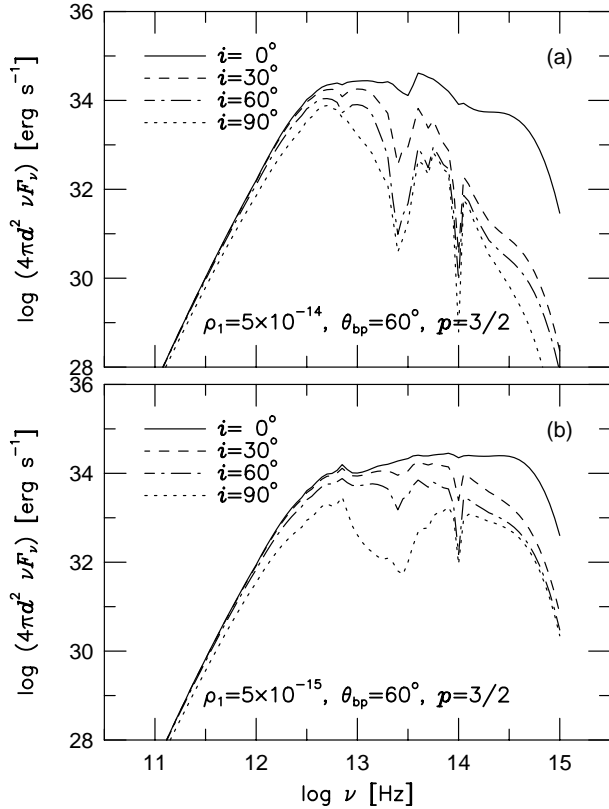


Fig. 8. Dependence of the SED on the reference density ρ_1 . (a) SEDs for a model with $\rho_1 = 5.0 \times 10^{-14} \text{ g cm}^{-3}$, $\theta_{\text{bp}} = 60^\circ$, and $p = 3/2$. (b) SEDs for a model with $\rho_1 = 5.0 \times 10^{-15} \text{ g cm}^{-3}$, $\theta_{\text{bp}} = 60^\circ$, and $p = 3/2$.

3.3. Dependence on the Halo Density Distribution

As illustrated in the previous subsection, the mid- to far-infrared portion of the SED is not sensitive to disk accretion. We therefore examine how the flat infrared spectrum depends on the assumed halo density distribution using models without disk accretion. We first test the sensitivity of the SED to the size of the bipolar lobes. Figure 7a shows SEDs for a model with the opening half-angle of the bipolar holes being $\theta_{\text{bp}} = 30^\circ$. The other parameters for the halo density distribution are the same as those of the standard model, i.e., $\rho_1 = 10^{-14} \text{ g cm}^{-3}$ and $p = 3/2$. Compared with the standard model having $\theta_{\text{bp}} = 60^\circ$, the emergent flux is considerably reduced at optical and near-infrared wavelengths when viewed at $i \geq 30^\circ$, because less optical and near-infrared light can escape from the central star through the bipolar holes. This means that more energy from the central star is used to heat the outer region of the disk. As a result, the mid- to far-infrared flux increases slightly, compared with the standard model. However, the effect of narrowing the opening half-angle of the bipolar holes may be compensated by reducing ρ_1 . Figure 7b shows SEDs for a model with a lower halo density: $\rho_1 = 5 \times 10^{-15} \text{ g cm}^{-3}$, $\theta_{\text{bp}} = 30^\circ$, and $p = 3/2$. As with the standard model, this

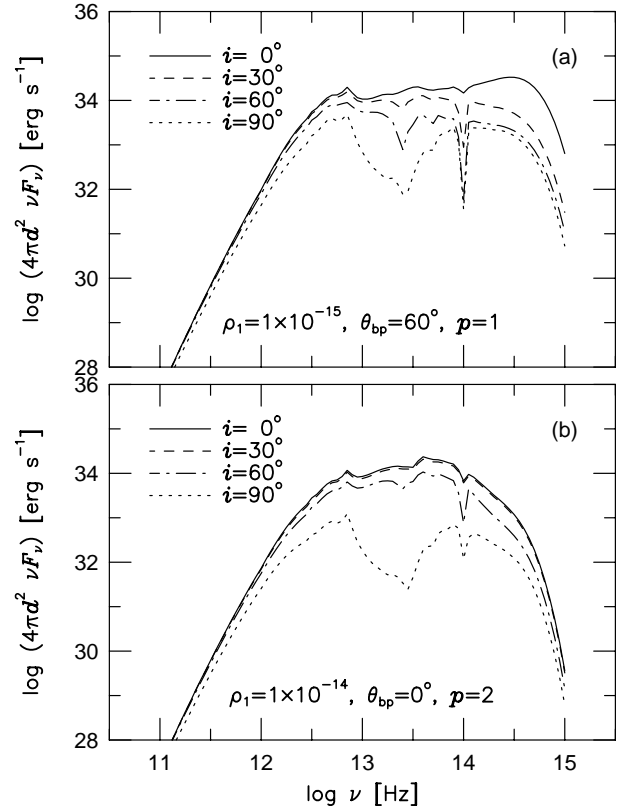


Fig. 9. Dependence of the SED on the power-law index, p . (a) SEDs for a model with $p = 1$, $\rho_1 = 1.0 \times 10^{-15} \text{ g cm}^{-3}$, and $\theta_{\text{bp}} = 60^\circ$. (b) SEDs for a model with $p = 2$, $\rho_1 = 1.0 \times 10^{-14} \text{ g cm}^{-3}$, and $\theta_{\text{bp}} = 0^\circ$.

model also produces flat infrared spectra when the viewing angle is $0^\circ \leq i \leq 60^\circ$. However, some differences are found in the SED. The absorption feature near $10 \mu\text{m}$ is shallower due to the reduced halo density, and the slope of the SED is more steep from the near-infrared to the optical.

Secondly, we examine how the halo density affects the SED. In figures 8a and 8b, model SEDs are shown for $\rho_1 = 5 \times 10^{-14}$ and $5 \times 10^{-15} \text{ g cm}^{-3}$, respectively. For both models, we adopt $\theta_{\text{bp}} = 60^\circ$ and $p = 3/2$. The model with a higher halo density, $\rho_1 = 5 \times 10^{-14} \text{ g cm}^{-3}$, shows relatively narrow SEDs when viewed at $i > 0$, and the peak of the SED occurs in the far-infrared. The emergent flux steeply declines from the near-infrared to the optical, because light from the hot inner regions is highly extinguished by the dense halo and only a small amount of scattered photon can escape the halo. Thus, this model is not classified as a “class II” object with flat infrared spectrum unless it is observed precisely pole-on. On the other hand, a model with a lower halo density, $\rho_1 = 5 \times 10^{-15} \text{ g cm}^{-3}$, still produces flat SEDs at a wide range of viewing angles, $\sim 30^\circ - 60^\circ$.

Finally, we examine the dependence of SEDs on the power-law index, p . A molecular cloud core which collapses to form a star and a disk is expected to be ro-

tating. At later stages of the collapse, infalling material lands onto the equatorial plane, rather than onto the central star. Thus, the halo density is reduced inside the centrifugal radius, and it decreases more slowly with the radius than spherically symmetric cases. We then consider a model with $p = 1$, $\rho_1 = 10^{-15} \text{ g cm}^{-3}$, and $\theta_{\text{bp}} = 60^\circ$. As shown in figure 9a, this model also produces flat infrared spectra at viewing angles of $i \sim 30^\circ - 60^\circ$. Compared with the standard model, it emits more optical flux, because the halo density is lower in the innermost region, so that more optical light escapes the halo.

If the central star drives a stellar wind with constant velocity and mass outflow rate, a power law, $\rho \propto r^{-2}$, is appropriate for the halo density distribution. Figure 9b shows SEDs for a model with $p = 2$, $\rho_1 = 10^{-14} \text{ g cm}^{-3}$, and $\theta_{\text{bp}} = 0^\circ$. Because the slope of the SEDs is positive in the infrared, $p = 2$ is not favored by the flat spectrum.

4. Discussion

4.1. Origin of the Flat Spectrum

The present results show that the disk-halo model can reproduce the overall spectral shape of typical flat-spectrum T Tauri stars. In our model, the mid- to far-infrared excesses of flat-spectrum T Tauri stars originate from the disk, rather than from the halo. The halo needed to heat the disk can be as compact as the disk, itself, and we suggest that a reflection nebula often associated with a T Tauri star is an observational counterpart of the halo. The reflection nebula probably corresponds to the inner part of a remnant of an infalling envelope. The disk-halo model is therefore consistent with the notion that the flat-spectrum T Tauri stars are in a transitional stage from protostars to T Tauri stars (Hayashi et al. 1993).

In contrast with the disk-halo model, the infalling envelope model of Calvet et al. (1994) explains the mid- to far-infrared excesses by the emission from infalling envelopes. Indeed, observations of molecular line emission have revealed extended, disk-like envelopes associated with several flat-spectrum T Tauri stars (Hayashi et al. 1993; Kitamura et al. 1996a; Momose et al. 1996). However, recent high-resolution observations have shown that the continuum emission at submillimeter and millimeter wavelengths originates entirely from a compact ($\lesssim 100 \text{ AU}$) region, suggesting that the extended ($\sim 1000 \text{ AU}$) envelopes traced by molecular line emission do not contribute to the submillimeter and millimeter emission (Lay et al. 1994; Kitamura et al. 1996b; Looney et al. 2000). Since infrared emission originates from warmer regions than submillimeter and millimeter emission, it is quite unlikely that the extended envelopes contribute to the infrared emission. Hence, the mid- to far-infrared excesses of flat-spectrum T Tauri stars should also originate from a compact region. The disk-halo model produces emission at any wavelength from a compact region, and therefore is more consistent with this observational constraint than the infalling envelope model.

If the mid- to far-infrared excesses of flat-spectrum T Tauri stars are to be explained by the emission arising

at 100–1000 AU in their infalling envelopes (Calvet et al. 1994), they should have been surrounded by sufficient amount of infalling material at a radius of 100–1000 AU as protostars are. Growing observational evidence, however, indicates that at these radii the amount of infalling material around flat-spectrum T Tauri stars is much less than that around embedded protostars (Ohashi et al. 1991, 1996), suggesting that the amount of infalling material inside 100–1000 AU around the central sources decreases during the course of evolution from protostars to T Tauri stars. Dispersing motion in the envelopes has actually been observed for T Tau (Momose et al. 1996) and DG Tau (Kitamura et al. 1996a). HL Tau is suggested to be situated in the bubble wall, which is an expanding shell with XZ Tau being the closest known source to the center (Welch et al. 2000). In addition, Momose (1998) showed that envelopes around flat-spectrum T Tauri stars are less centrally condensed than those around protostars. These results imply that infalling material around 100–1000 AU has been dissipated away, or has accreted onto the central star/disk system.

In our view, the inner parts of the envelopes around flat-spectrum T Tauri stars are still optically thick to stellar radiation, although they do not have sufficient mass to produce the mid- to far-infrared excesses. For instance, the visual extinction toward HL Tau was estimated to be $A_V > 22 \text{ mag}$ (Stapelfeldt et al. 1995), which is comparable to that in our calculations. In the disk-halo model, visual extinction varies widely depending on the viewing angle as well as on the density distribution in the halo; thus, our model can explain the flat spectrum for objects with various visual extinction values. The detailed structure of the halo, however, cannot be predicted by the analysis of SEDs, because the halo structure is not unique to give the observed flat spectra. Obviously, to solve the degeneracy, further observational information is needed on the structure within 100 AU. High-resolution observations of the scattered light in the near-infrared may provide crucial information on the structure of the disk and halo (Close et al. 1997). We will report on a comparison between the disk-halo model and near-infrared observations in a future paper.

4.2. Effects of Shock Heating

If the halo is an innermost part of the infalling envelope, the envelope gas should shock the disk surface. This shock heating could be an important energy source which our analyses do not take into account. To clarify quantitatively how shock heating modifies the SED in the infrared region, detailed radiation hydrodynamics calculations will be needed. Although such analysis is beyond the scope of this paper, we can discuss that the amount of energy released at the disk surface by the shock would not be sufficient to modify the SED obtained in our standard model.

Suppose that envelope gas freely falls onto the disk along a ballistic orbit, the initial cloud core is spherically symmetric and uniformly rotating, the infall is initiated by the expansion wave (Shu 1977), and the gas joins a Keplerian disk behind the shock. The amount of energy

dissipated at shock per unit mass is $GM_*/2R$. We denote by $F(R)$ the mass flux from the envelope on the disk at radius R , which is given by equation (2.1) in Nakamoto and Nakagawa (1994). If we adopt $\dot{M} = 0.9 \times 10^{-5} M_\odot \text{ yr}^{-1}$ (Hayashi et al. 1993), $R_{\text{out}} = 100 \text{ AU}$ (R_{out} is denoted by R_d in Nakamoto, Nakagawa 1994), and $M_* = 0.5 M_\odot$, the energy generation rate due to shock heating at the disk surface per unit area, ε_s , is given by

$$\begin{aligned} \varepsilon_s &= \frac{1}{2} \frac{GM_*}{R} F(R) \\ &= \frac{1}{2} \frac{GM_*}{R_{\text{out}}} \left(\frac{R_{\text{out}}}{R} \right)^2 \frac{1}{\sqrt{1 - R/R_{\text{out}}}} \\ &= 0.45 \left(\frac{R}{100 \text{ AU}} \right)^{-2} (1 - R/100 \text{ AU})^{-1/2} \\ &\quad \text{erg cm}^{-2} \text{ s}^{-1}. \end{aligned} \quad (8)$$

If there were no irradiation from the central star, the disk surface would be heated by shock heating to the temperature

$$\begin{aligned} T_{\text{eff}} &= (\varepsilon_s / \sigma_B)^{1/4} \\ &= 94 \left(\frac{R}{1 \text{ AU}} \right)^{-1/2} (1 - R/100 \text{ AU})^{-1/8} \text{ K}, \end{aligned} \quad (9)$$

which is much lower than the temperature obtained by our standard model including irradiation (see figure 3). Therefore, it seems that shock heating at the surface of the disk has only a negligible effect on the observed SED from the flat-spectrum T Tauri disk.

5. Conclusions

1. We have shown that disks heated by the scattering and reprocessing of the stellar radiation through the halo can have flat infrared spectra.
2. Local viscous heating is not sufficient to produce large mid- to far-infrared emission from the disk if we consider a reasonable rate of mass accretion in disks around classical T Tauri stars. However, the accretion energy released in the innermost region of the star/disk system is transported by radiation through the halo to heat the outer region of the disk, resulting again in a flat spectrum.
3. We examined the sensitivity of the SED to the assumed halo structure, and found that density distributions with a power-law index $\leq 3/2$ can provide the backwarming needed for flat infrared spectra. However, we have found that it is difficult to constrain the halo structure only from the SED in the infrared.
4. We have discussed that the halo will be observed as a reflection nebula often associated with a T Tauri star, indicating that it is the inner part of a remnant of an infalling envelope. A more detailed test of the model will be made by comparisons with imaging observations of near-infrared scattered light.

We are grateful to M. Hayashi and M. Umemura for

valuable discussions. We also thank an anonymous referee for suggestions which improved the paper. The computations were performed on CP-PACS at the Center for Computational Physics in University of Tsukuba, and on the Fujitsu VPP300/16R at the Astronomical Data Analysis Center of the National Astronomical Observatory, Japan. TN was partially supported by the Grant-in-Aid for Scientific Research on Priority Areas (10147105) and for Scientific Research (10740093) of the Ministry of Education, Culture, Sports, Science, and Technology, Japan.

References

- Adams, F. C., Lada, C. J., & Shu, F. H. 1988, *ApJ*, 326, 865
Adams, F. C., & Shu, F. H. 1986, *ApJ*, 308, 836
Beckwith, S. V. W., Sargent, A. I., Chini, R. S., & Güsten, R. 1990, *AJ*, 99, 924
Bertout, C., Basri, G., & Bouvier, J. 1988, *ApJ*, 330, 350
Butner, H. M., Natta, A., & Evans, N. J., II 1994, *ApJ*, 420, 326
Calvet, N., Hartmann, L., Kenyon, S. J., & Whitney, B. A. 1994, *ApJ*, 434, 330
Chiang, E. I., & Goldreich, P. 1997, *ApJ*, 490, 368
Close, L. M., Roddier, R., Northcott M. J., Roddier, C., & Graves, J. E. 1997, *ApJ*, 478, 766
D’Alessio, P., Calvet, N., & Hartmann, L. 1997, *ApJ*, 474, 397
Hayashi, C., Nakazawa, K., & Nakagawa, Y. 1985, in *Protostars and Planets II*, ed. D. C. Black & M. S. Matthews (Tucson: Univ. Arizona Press), 1100
Hayashi, M., Ohashi, N., & Miyama, S. M. 1993, *ApJ*, 418, L71
Kenyon, S. J., Calvet, N., & Hartmann, L. 1993, *ApJ*, 414, 676
Kenyon, S. J., & Hartmann, L. 1987, *ApJ*, 323, 714
Kitamura, Y., Kawabe, R., & Saito, M. 1996a, *ApJ*, 457, 277
Kitamura, Y., Kawabe, R., & Saito, M. 1996b, *ApJ*, 465, L137
Kusaka, T., Nakano, T., & Hayashi, C. 1970, *Prog. Theor. Phys.* 44, 1580
Lay, O. P., Carlstrom, J. E., Hills, R. E., & Phillips, T. G. 1994, *ApJ*, 434, L75
Lin, D. N. C., Hayashi, M., Bell, K. R., & Ohashi, N. 1994, *ApJ*, 435, 821
Looney, L. W., Mundy, L. G., & Welch, W. J. 2000, *ApJ*, 529, 477
Lynden-Bell, D., & Pringle, J. E. 1974, *MNRAS*, 168, 603
Masunaga, H., Miyama, S. M., & Inutsuka, S. 1998, *ApJ*, 495, 346
Miyake, K., & Nakagawa, Y. 1993, *Icarus*, 106, 20
Momose, M. 1998, PhD thesis, The Graduate University for Advanced Studies
Momose, M., Ohashi, N., Kawabe, R., Hayashi, M., & Nakano, T. 1996, *ApJ*, 470, 1001
Nakamoto, T., & Nakagawa, Y. 1994, *ApJ*, 421, 640
Natta, A. 1993, *ApJ*, 412, 761
Ohashi, N., Hayashi, M., Kawabe, R., & Ishiguro, M. 1996, *ApJ*, 466, 317
Ohashi, N., Kawabe, R., Hayashi, M., & Ishiguro, M. 1991, *AJ*, 102, 2054
Sargent, A. I., & Beckwith, S. V. W. 1991, *ApJ*, 382, L31
Shu, F. H. 1977, *ApJ*, 214, 488
Stapelfeldt, K. R., Burrows, C. J., Krist, J. E., Trauger, J. T., Hester, J. J., Holtzman, J. A., Ballester, G. E., Casertano, S., Clarke, J. T. Crisp, D., Evans, R. W., Gallagher, J. S.,

- III, Griffiths, R. E., Hoessel. J. G., Mould, J. R., Scowen, P. A., Watson, A. M., & Westphal, J. A. 1995, ApJ, 449, 888
- Stone, J. M., Mihalas, D., & Norman, M. L. 1992, ApJS, 80, 819
- Strom, K. M., Strom, S. E., Edwards, S., Cabrit, S., & Skrutskie, M. F. 1989, AJ, 97, 1451
- Welch, W. J., Hartmann, L., Helfer, T., & Briceño, C. 2000, ApJ, 540, 362